TECHNOLOGY • RESEARCH HIGHLIGHTS • VISIONS • SCIENCE

114

Method for estimating wind turbine production losses due to icing

Ville Turkia | Saara Huttunen | Tomas Wallenius

VTT TECHNOLOGY 114

Method for estimating wind turbine production losses due to icing

Ville Turkia, Saara Huttunen & Tomas Wallenius

ISBN 978-951-38-8041-5 (URL: http://www.vtt.fi/publications/index.jsp)

VTT Technology 114

ISSN-L 2242-1211
ISSN 2242-122X (verkkojulkaisu)

JULKAISIJA – UTGIVARE – PUBLISHER

VTT
PL 1000 (Tekniikantie 4 A, Espoo)
02044 VTT
Puh. 020 722 111, faksi 020 722 7001

VTT
PB 1000 (Teknikvägen 4 A, Esbo)
FI-02044 VTT
Tfn +358 20 722 111, telefax +358 20 722 7001

VTT Technical Research Centre of Finland
P.O. Box 1000 (Tekniikantie 4 A, Espoo)
FI-02044 VTT, Finland
Tel. +358 20 722 111, fax + 358 20 722 7001

Technical editing Tarja Haapalainen

Method for estimating wind turbine production losses due to icing

Menetelmä jäätymisen aiheuttamien tuuliturbiinin tuotantotappioiden arviointiin. **Ville Turkia, Saara Huttunen & Tomas Wallenius.** Espoo 2013. VTT Technology 114. 38 p.

Abstract

Atmospheric icing causes production losses to wind turbines, poses a risk of ice throw and increases dynamic loading of wind turbine which might reduce the lifetime of turbine components. These effects are qualitatively widely known but not quantitatively. In order to estimate effects of icing to power production of a typical 3 MW wind turbine, a simulation based study was made.

Three rime ice cases were selected with the meteorological conditions typical for Finnish climate. Conditions were the same for each case. The lengths of the icing events were varied to represent different phases of an icing event; beginning of icing, short icing event and long lasted icing event. Thus, three different ice masses accreted on a wind turbine blade were simulated. Accretion simulations were performed with a VTT inhouse code TURBICE. The aerodynamical properties of the iced profiles were modelled using computational fluid dynamics (CFD) with ANSYS FLUENT flow solver. As a result, lift and drag coefficients were drawn as a function of an angle of attack. Small-scale surface roughness effect on drag coefficient was determined analytically. Finally, the power curves were generated with FAST software for the clean wind turbine and for the same turbine with the different ice accretions.

The results showed relatively large impact of small-scale surface roughness on power production. In the beginning of an icing event, where ice causes basically only increased surface roughness, power production was discovered to reduce by approximately 17 % below rated wind speeds compared to the no-ice case. As the ice mass was increased, production reduction was 18 % for short icing event and 24 % for long lasted icing event. However, the relative reduction was smaller than in the beginning of icing, mainly due to the small-scale surface roughness that remained at the same level. The results indicate that the surface roughness is crucial to take into account when defining the aerodynamic penalty caused by icing of wind turbine blades. The generated power curves for iced up wind turbine in this study estimate higher power production than can be expected from the observations in real life. This is caused by the less complex ice shapes resulting from simulating only rime ice conditions.

The results of this study were used in the Finnish Icing Atlas *(2012)*, where time dependent numerical weather simulations were carried out to calculate icing conditions and energy production losses. The results were also used in ICEWIND project for production loss estimation process.

Keywords icing, wind turbine, production loss, simulation, rime ice, icing atlas

Menetelmä jäätymisen aiheuttamien tuuliturbiinin tuotantotappioiden arviointiin

Method for estimating wind turbine production losses due to icing. **Ville Turkia, Saara Huttunen & Tomas Wallenius.** Espoo 2013. VTT Technology 114. 38 s.

Tiivistelmä

Tuulivoimaloiden lapoihin kertyvä jää aiheuttaa tuulivoimaloille tuotantotappioita, aiheuttaa jäänlentoriskin ja kasvattaa tuulivoimalan komponenttien väsymiskuormia, jotka voivat johtaa komponenttien eliniän lyhenemiseen. Nämä jäätämisen haittavaikutukset tunnetaan laajalti, mutta niiden suuruutta on ollut vaikea arvioida. Tässä tutkimuksessa arvioidaan jään aiheuttamaa tehon alenemaa tyypilliselle 3 MW tuulivoimalalle simuloinnin keinoin.

Kolme Suomen ilmastolle tyypillistä jäätämistapausta valittiin edustamaan oleellisinta osaa tuotantotappioita aiheuttavista jäätämistilanteista. Meteorologiset suureet olivat samat jokaiselle tapaukselle, mutta jäätämistilanteiden kestoa kasvatettiin, jotta voitiin kuvata jäätämisen alkuvaihe sekä lyhyehkö ja pitkään jatkunut jäätämistilanne. Nämä kolme jäätämistilannetta simuloitiin VTT:n omalla TURBICE-ohjelmalla. Aikaansaatujen kolmen jäämuodon aerodynaamiset ominaisuudet mallinnettiin laskennallisen virtausmekaniikan (CFD) keinoin käyttäen ANSYS FLUENT -ohjelmaa. Pinnankarheuden vaikutus vastukseen määriteltiin erikseen analyyttisellä menetelmällä. Lopulta esimerkkituulivoimalan tehokäyrät simuloitiin FAST-ohjelmalla puhtaalle tuulivoimalalle ja kolmelle jäätymistapaukselle.

Tulokset osoittivat pinnankarheuden vaikuttavan tehontuotantoon verrattain paljon. Jäätämisen alkuvaiheessa käytännössä ainoastaan tuulivoimalan lavan pinnankarheus muuttuu, mikä johti noin 17 % tehon alenemaan toimittaessa alle nimellistuulennopeuden. Jään massan kasvaessa tehon alenema kasvoi edelleen 18 %-yksikköön lyhyehköllä jäätämistapauksella. Pitkään jatkuneella jäätämistapauksella tehon alenema oli 24 %, mutta muutos oli suhteellisesti pienempää, sillä pinnankarheus pysyi samansuuruisena. Tulokset osoittavat, että pinnankarheuden huomioon ottaminen on erittäin tärkeää määriteltäessä jäätyneiden tuulivoimalan lapojen aerodynaamisia ominaisuuksia. Tässä tutkimuksessa lasketut tehon alenemat ovat pienempiä verrattuna joihinkin todellisiin havaintoihin, sillä jäämuodot laskettiin vain huurrejäätapauksille, joissa jään muodot eivät ole yhtä monimutkaisia kuin ne tosielämässä voivat olla.

Tämän työn tuloksena saatuja tehokäyriä käytettiin Suomen Jäätämisatlaksessa, jossa numeerisella sääennusteohjelmalla simuloitiin sääolosuhteita ja laskettiin jäätämisolosuhteita sekä jäätämisen aiheuttamia tappioita energiantuotantoon. Tuloksia hyödynnettiin myös ICEWIND-projektissa tuotantotappioiden arvioinnissa.

Avainsanat icing, wind turbine, production loss, simulation, rime ice, icing atlas

Preface

This publication describes the generation of the reduced power curves for iced-up typical 3 MW wind turbine, including the modelling of the ice accretions on wind turbine rotor blades and evaluating aerodynamic effects of ice. Results were used in Icewind project and to build-up Finnish Icing Atlas, which was published in combination with Finnish Wind Atlas in early 2012 by Finnish Meteorological Institute. Most of the work was done in 2010–2012.

Contents

List of symbols and abbreviations

CC	Cold Climate
CFD	Computational Fluid Dynamics
FMI	Finnish Meteorological Institute
LWC	Liquid Water Content
MBS	Multi Body Simulation, simulations of dynamic behavior of interconnected bodies
MVD	Mean Volume Diameter, parameter describing water droplet size distribution in coulds

C_D	Drag coefficient
$C_{D_{iced}}$	Drag coefficient of iced profile
ΔC_D	Correction factor of drag coefficient
C_L	Lift coefficient
c	Chord
k	Roughness height
P	Power

1. Introduction

Cold climate sites around the World offer large wind energy potential in demanding winter climates. Based on the World Market Update 2010 *(BTM Consult 2011)* and NREL report *(US Department of Energy 2012)*, the installed wind power capacity only for regions with high likelihood of extended cold climate operation in Scandinavia, Switzerland, Canada, northern parts of USA, and China were conservatively estimated to be 20 GW. Wind turbines in cold climates (CC) are exposed to icing conditions and/or low temperatures outside the design limits of standard wind turbines. Icing, more particularly in-cloud icing (later only icing), can have significant effect on wind turbine power production. In addition to the decreased power production, icing causes risk of ice throw and increases dynamic loading of a wind turbine which might lead to a premature failure of turbine components. Ice build-up on wind turbine blades also icreases noise levels of turbines.

In order to help wind energy project developers to take icing into account in site assessment phase, icing maps are needed. Icing maps, which are usually created using computer modelling, give a first estimate of icing conditions at the potential site. These estimates incorporate relatively big uncertainties due to the complexity of the icing phenomena and resulting simplifications done in computer modelling. Because of the uncertainties in computer model based icing maps, icing has to be measured in the site assessment phase and compared to a long term average, if available, to acquire enough information about the site icing conditions. Based on the site assessment, the needed counter measures against the adverse effects of icing can be planned.

Wind energy production targets among other renewables in Finland for 2020 have been set to a high level compared to the present state, where wind energy contributed 0,6 % of the consumed electricity in the end of 2011 according to the Finnish wind power statistics *(VTT 2012)*. To boost up the development of the wind power capacity from 200 MW up to 2000 MW, a feed-in tariff has been set up. To help the wind energy development in Finland, Finnish Icing Atlas has been constructed in connection to the Finnish Wind Atlas.

The Finnish Icing Atlas was constructed in collaboration between VTT and Finnish Meteorological Institute (FMI). FMI conducted the weather and icing modelling. The numerical weather modelling for the Icing Atlas was done with AROME weather model where icing model based on the ISO standard *(ISO 12494 2001)*

was used to calculate the accumulated ice mass on a stationary cylinder (later standard cylinder) in each weather conditions. VTT conducted a three phase modelling of power performance behaviour of a wind turbine under icing conditions. In the first phase, different ice accretion cases on wind turbine rotor blades were simulated. Then the aerodynamic properties of the iced up airfoils for each case were modelled by computational fluid dynamics (CFD). In the third phase a set of power curves were generated for the iced up wind turbine cases.

The generation of the reduced power curves, including the modelling of ice accretion on wind turbine rotor blades and the aerodynamic effects of ice, is described in this report.

2. Process for modelling production losses due to icing

Ice accretion on wind turbine rotor blades causes production losses, as the ice build-ups degrade the aerodynamic properties of the blades. On rotating wind turbine ice builds up mostly on the leading edge of the blades and the effects of ice depend on the amount and the shape of the ice. The effect of ice on wind turbine power production was assessed as follows:

1) Three different ice formations on wind turbine blades were created using TURBICE software, a numerical ice accretion simulation tool for wind turbines *(Makkonen et al. 2001)*. Detailed description of ice accretion simulations is in Chapter 3.

2) Aerodynamic properties of the iced wind turbine blades, created in step 1, were analysed with computational fluid dynamic (CFD) analysis. CFD analysis is described in Chapter 4.

3) Power curves of iced up wind turbine were simulated using wind energy specific multibodydynamic (MBS) software and the aerodynamics of iced up blades, from step 2, as input. See more in Chapter 5.

4) The power curves of iced wind turbine, from step 3, were linked to time dependent weather conditions resulting similar ice formations as were created in step 1. In principal the reduced power curves were linked to icing conditions so that ice masses on the rotor blade were considered and a relation to ice mass on a stationary standard cylinder in weather model was established. More detailed description of the linking can be found from Section 2.1

The whole simulation based process of production loss estimation in connection to numerical weather modelling is illustrated in Figure 1.

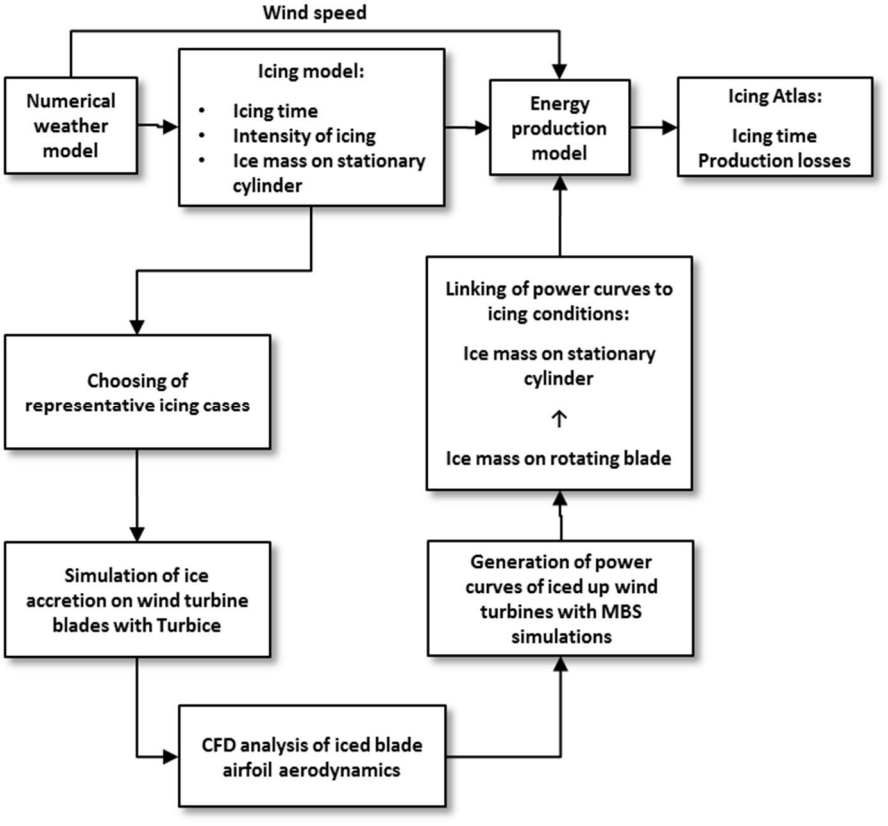

Figure 1. Process overview of power production loss estimation.

2.1 Relation between stationary cylinder and rotating wind turbine blade

Ice accretion is modelled in numerical weather prediction models commonly using the model described in ISO 12494 *(2001)* standard, which defines the ice accretion to the cylinder. Therefore, a relation between the standard stationary cylinder and a rotating wind turbine blade was determined. The main equation describing ice accretion rate to an object is

$$\frac{\mathrm{dM}}{dt} = \alpha_1 \cdot \alpha_2 \cdot \alpha_3 \cdot w \cdot v \cdot A, \qquad \left[\frac{kg}{s}\right] \tag{1}$$

where A (m^2) is the cross-sectional area of the object with respect to the direction of the flow velocity vector, w (kg/m^3) is the mass concentration of the particles, v (m/s) is the relative velocity of the flow, and the α_1, α_2, and α_3 are correction factors describing the droplet impingement to the object and freezing varying between 0…1.

Comparison of ice masses on the cylinder and on the blade were done to a blade section at the radius of 85 % of total radius, because that radius has the biggest contribution to the power production of a turbine *(Burton et al. 2001)*. It was also considered that the section at the radius of 85 % of total radius represents the average ice accretion on a blade.

Due to the numerous variables affecting the icing of a wind turbine rotor blade, it was decided to simplify the problem by choosing one weather condition that was used to establish the relation between the icing of the moving wind turbine rotor blade and the icing the standard cylinder. The most dominant variable in ice accretion is the relative wind speed, as described in equation (1). By scaling down NREL 5 MW turbine and using the original rotational speed in relation to wind speed, 12.4 rpm rotor rotational speed was achieved with a wind speed of 7.5 m/s and these values were chosen for simulation. The air temperature, -5 °C, was selected so that the resulting ice type in every case would be rime ice[1].

Homola et al. *(2010)* showed that supercooled water droplets, which cause the in-cloud icing, cause the same amount of degradation in lift and drag coefficient when mean volume diameter (MVD) is 17 μm or higher. In this study MVD were chosen to be 25 μm, in order to achieve reasonable computing time for ice accretion calculations in TURBICE. Liquid water content (LWC) of air was chosen to be 0.2 g/m^3, which is typical value. All the input values are presented in Table 1.

The relation between ice masses on the standard cylinder and the wind turbine blade in the same weather conditions was represented by the factor k, as illustrated in Figure 2. The factor k was calculated by dividing the ice mass on the blade with the ice mass on the cylinder. Calculation of the parameter k was based on Turbice simulations with input values as described above. Temperature, wind speed and droplet size were varied around the specified values and an average value of k = 20 was obtained. In principal, this means that in the same icing and wind conditions a rotating wind turbine blade collects approximately 20 times more ice per meter than the stationary cylinder.

[1] Rime ice is the most common type of in-cloud icing and often forms vanes on the windward side of objects for example on rotating wind turbine blade. Another typical ice type is glaze ice, which causes more complex ice shapes to wind turbine blades. Glaze ice forms typically in temperatures close to 0°C whereas rime ice forms more likely in lower temperatures. More information about different ice types can be found from the ISO 12494:2001 standard.

Table 1. Input values used in Turbice simulation in forming cylinder-blade –relation.

Parameter	**Value**	**Unit**
Wind speed (for blade)	7.5	m/s
Rotor rotational speed (for blade)	12.4	RPM
Total speed for cylinder	7.5	m/s
Temperature	-5	°C
Droplet size	25	µm
Liquid water content (LWC)	0.2	g/m^3
Air pressure	96	kPa
Simulation time	60	min

Figure 2. Parameter k links the accreted ice mass on cylinder to the ice mass on blade.

3. Ice accretion simulations on wind turbine rotor blades

3.1 Simulation cases

To reproduce adequate ice shapes accreting on wind turbine rotor blade, ice accretion simulations were carried out using TURBICE software, which is a numerical ice accretion simulation software based on panel method. Due to the large number of parameters, complexity and limitations in softwares and information available, some simplifications had to be done.

Three icing cases denoted as *start of icing, light icing* and *moderate icing* were determined to represent the icing distribution in Finland as calculated in the Finnish Icing Atlas. The icing distribution is presented in Figure 3. In the Finnish Icing Atlas it was considered that 10 g/m of ice on the cylinder was the smallest amount of icing to be taken into account. It corresponds to an amount of ice on the rotor blade that could be expected to cause noticeable power decrease based on observations. The properties causing aerodynamic penalty for each icing case are presented in Table 2. The properties causing aerodynamic penalty are divided into three categories: small-scale surface roughness, large-scale surface roughness and ice geometry. Small-scale surface roughness represents the roughness on the surface of the ice, defined as sand-grain roughness. Large-scale roughness represents the larger bumpy structure of the accreted ice. Ice geometry itself represents the accumulated ice mass and volume that usually forms into a shape of a horn in the direction of the flow in rime ice situation or two horns, upwards and downwards of the blade's leading edge in glaze ice situation.

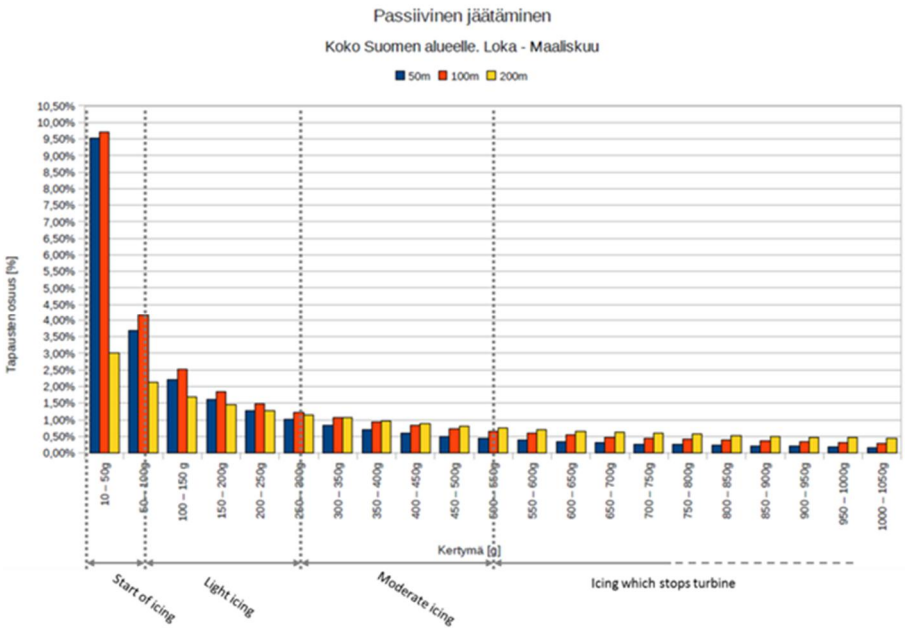

Figure 3. Icing distribution in Finland between October and November. X –axis describes the amount of accreted ice in kilograms and y –axis describes the share of each class in percentage of all classes. The chosen icing cases for turbine rotor blades are marked on the x –axis.

Table 2. Icing cases.

Icing case	Properties causing aerodynamic penalty
0 – No ice	Clean airfoil
1 – Start of icing	Small-scale roughness Large-scale roughness
2 – Light icing	Small-scale roughness Large-scale roughness A “dolphin nose” like rime ice geometry
3 – Moderate icing	Small-scale roughness Large-scale roughness Horn like rime ice geometry

Only outer third of the blade was considered iced, because it produces the most of the energy. As the ice accretion, blade and aerodynamic properties change by the blade radius, the blade tip part was divided into three sections as shown in Figure 4. Only Section 1 and Section 3 were modelled, because of limited resources. The Section 1 results were then applied also to the inner half of the Section 2 and the Section 3 results to the outer half of the Section 2 respectively.

The airfoil geometries, where ice was accreted, were selected in the middle of the sections 1 and 3 for each icing case.

NACA-64618 airfoil was used for simulation in all cases, because NACA 646xx airfoil is a commonly used profile in wind turbine blades, and 18 % is a typical value of a thickness ratio for the outer third of turbine blades. Blade chord and twist for each section were estimated by scaling the NREL 5 MW turbine rotor *(Jonkman et al. 2009)*.

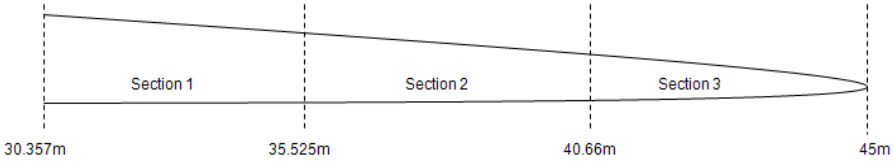

Figure 4. Blade tip definition for simulations. Radial distance is from the centre of rotation.

The different icing cases on the blade were created with TURBICE using constant weather conditions and parameters described in the Table 3, but varying time in order to simulate different durations of icing events. The icing event durations were 20, 200 and 600 simulation minutes for start of icing, light icing and moderate icing cases, respectively. The simulation times were chosen so that the icing cases cover all the icing classes presented in Figure 3. The wind speed was selected to be 7 m/s to represent typical operating wind speed during icing conditions. NREL 5 MW turbine was scaled down by assuming a constant tip speed, and a rotor rotational speed of 11.5 rpm was achieved. Air temperature was chosen to be -7 °C so that the resulting ice type is rime ice. These settings cause simplier ice shapes than what can be expected when temperature is closer to zero Celsius. Droplet size and liquid water content were chosen to represent typical icing conditions, as justified earlier in Section 2.1.

Table 3. Weather conditions and parameters for ice accretion simulations.

Parameter	Value	Justification
Wind speed	7 m/s	typical operating wind speed
Rotor rotational speed	11.5 rpm	calculated value
Air temperature	-7 °C	resulting ice type: rime
Droplet size distribution, mean volume diameter MVD	25 µm	typical in-cloud condition
Liquid water content LWC	0.2 g/m^3	typical in-cloud condition

3.2 Results

The simulated ice shapes were smoother than typical ice accretion on a wind turbine blade, because TURBICE software could not model the large-scale surface roughness. Therefore the ice shapes were modified to better represent real life situation with a more bumby and rough surface contour. An example of an ice accretion on a wind turbine blade is shown in Figure 5 and it was used, among other typical real life ice accretion photos, as a guideline to modify the contour of ice accretions. The ice accretions with general geometry from TURBICE and with roughened surface contour for blade section 1 for each icing case are shown in Figure 6. The ice shapes for section 3 were very similar. Ice masses for all simulation cases are presented in Table 4.

Figure 5. An example photo of an ice accretion.

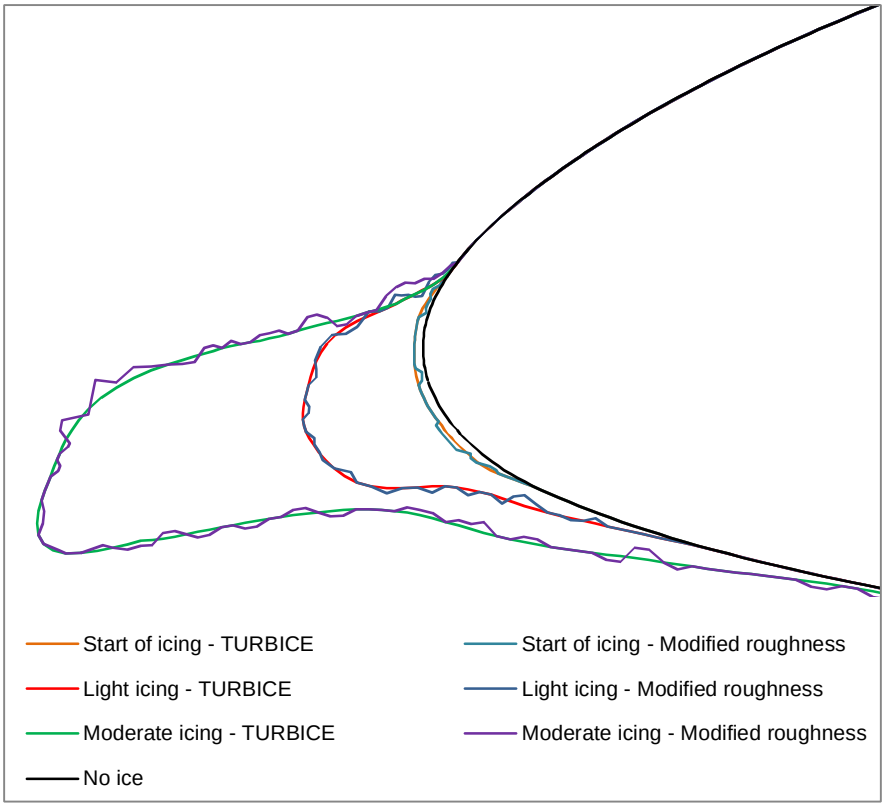

Figure 6. Original ice shapes created by TURBICE and large-scale surface roughness modified ice shapes for each icing case for Section 1.

Table 4. The representative ice masses of the blade sections in each case.

Case	Ice mass of Section 1 [kg/m]	Ice mass of Section 3 [kg/m]
0 – No ice	0	0
1 – Start of icing	0.2	0.3
2 – Light icing	2.5	3.5
3 – Moderate icing	7.1	9.4

4. Iced blade aerodynamics

CFD simulations were used to determine the lift and drag coefficients for the iced airfoils. Simulations were performed with ANSYS FLUENT. Ice shapes had bumpy structures and those bumps were regarded as large-scale surface roughness. Large-scale surface roughness was treated as a part of the airfoil geometry, and the grid was produced over the bumps. Additionally, the small-scale surface roughness, also referred to as sand-grain roughness, was determined by a separate method described by Shin et al. *(1994)*.

Initial testing for a clean NACA64618 airfoil revealed it would be challenging to model the small-scale surface roughness of the ice by CFD. Small-scale surface roughness on ice is relatively high. That prevented the use of a regular roughness parameter of ANSYS FLUENT, as the roughness was greater in height than the required height of the first cell on the wall. Wall functions were tested for avoiding this restriction, but this method proved not to be accurate enough for simulating the aerodynamic properties. The small-scale surface roughness effects were decided to be accounted for afterwards. This method will be described in more detail in Section 4.4.

4.1 Turbulence model for CFD

Two test cases were used to guide the selection of the appropriate turbulence model, grid and initial conditions. A literature reference *(Harold 2000)* was used, as it offered the ice shape geometries and experimental wind tunnel results of lift and drag coefficients together with pressure coefficient distribution along the upper and lower surfaces for different ice shapes for general aviation airfoil NLF-0414. More specifically, cases 622 and 623 *(Harold 2000)* were selected for comparison. Airfoil geometries provided by the reference were used to create the geometries and grids for CFD simulations, and different turbulence models were tested for gaining the best equivalence between the experimental and simulation results. Based on the two test cases, Spalart-Allmaras turbulence model was selected. It has also proved its efficiency for similar kind of simulations earlier *(Mortensen 2008)*. Although it has to be noted that the Spalart-Allmaras turbulence model is known to lack accuracy in modelling stall phenomenon.

4.2 Grid

C-shape grids were used with approximately 450000, 505000 and 540000 cells in Cases 1, 2 and 3, respectively, each count varying slightly by the blade section. Overall image of C-shape grid can be seen in Figure 7 and a close-up image of the distorted cells along the surface is presented in Figure 8. Grids presented here are only for blade section 1, as the geometry does not change much by the section. Grid-wisely challenging ice shapes can be seen in Figure 9, Figure 11 and Figure 13, for cases 1, 2 and 3, respectively. Quality of the cells remained satisfying while still maintaining a decent number of cells for optimizing the computation time. Y+ values on the airfoil surface can be seen to be in a range of 1 as show in Figure 10, Figure 12 and Figure 14, and that satisfies the requirements for turbulence model without wall functions.

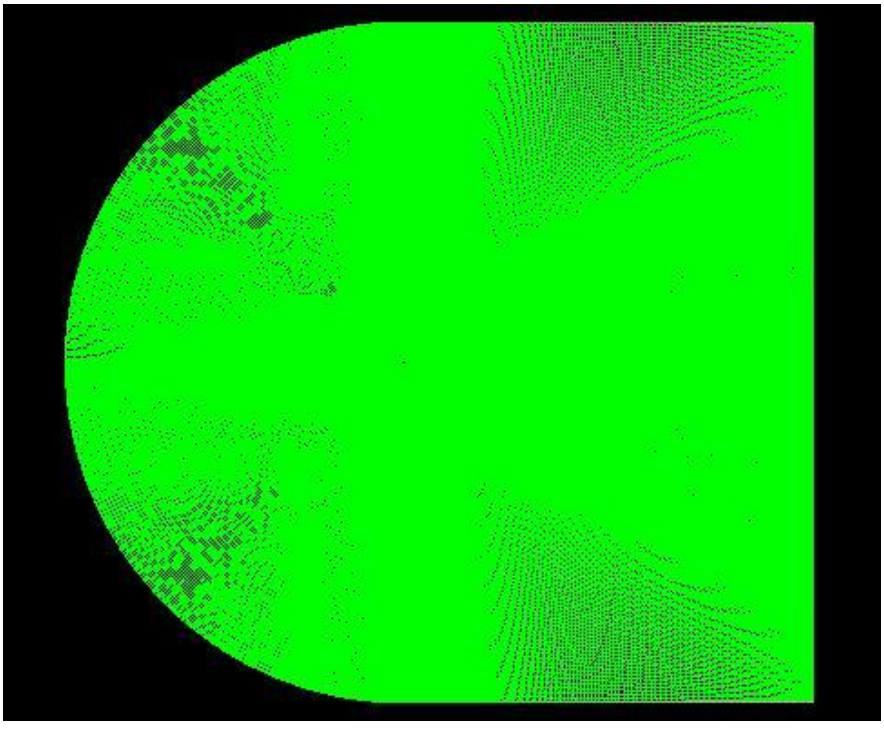

Figure 7. C-shape grid used in CFD calculations.

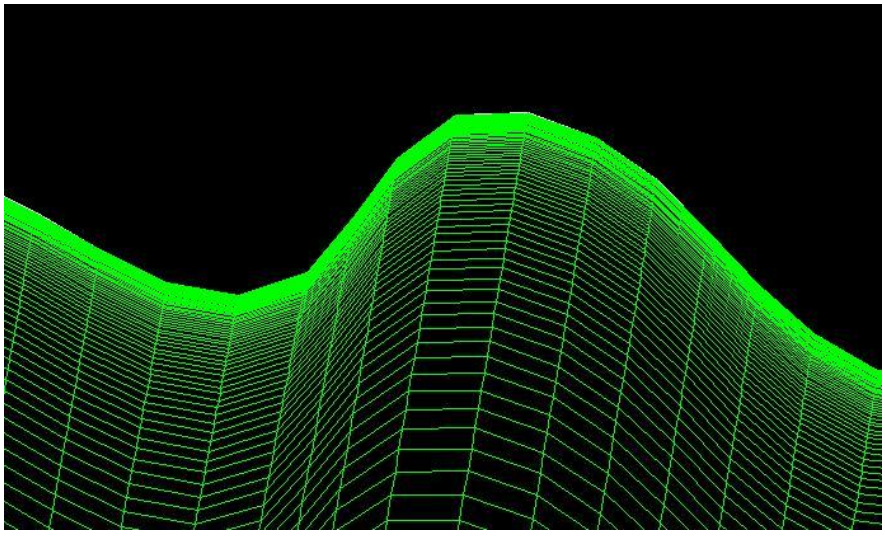

Figure 8. Close-up picture of the distorted grid in Case 3 section 1 with moderate rime ice geometry.

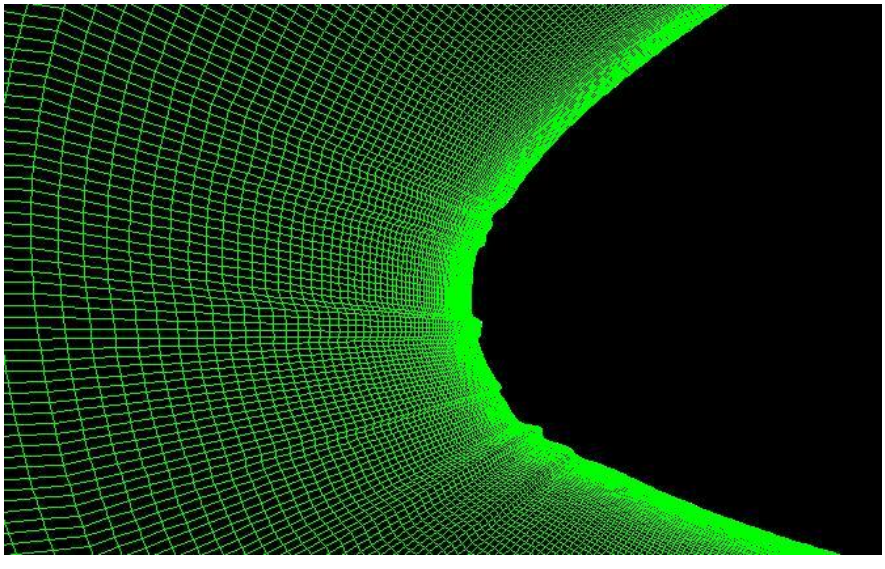

Figure 9. Grid on the leading edge of the airfoil in Case 1 for section 1.

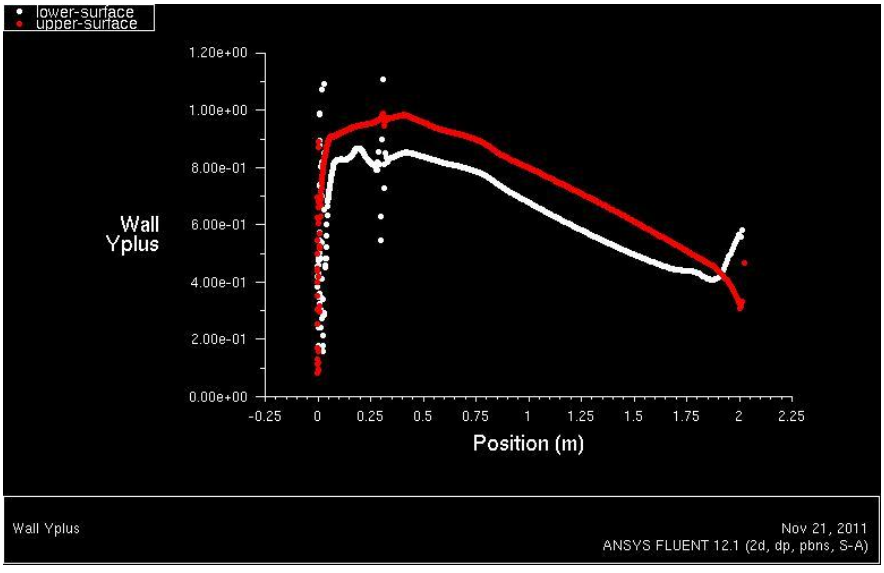

Figure 10. Wall y+ values on the airfoils upper and lower surfaces as a function of chord position in Case 1 for section 1.

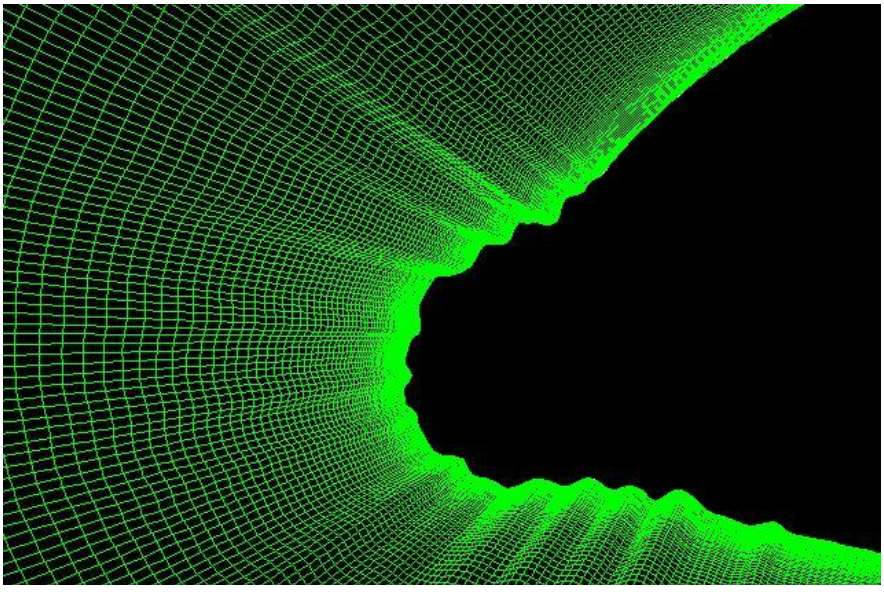

Figure 11. Grid on the leading edge of the airfoil in Case 2 for section 1.

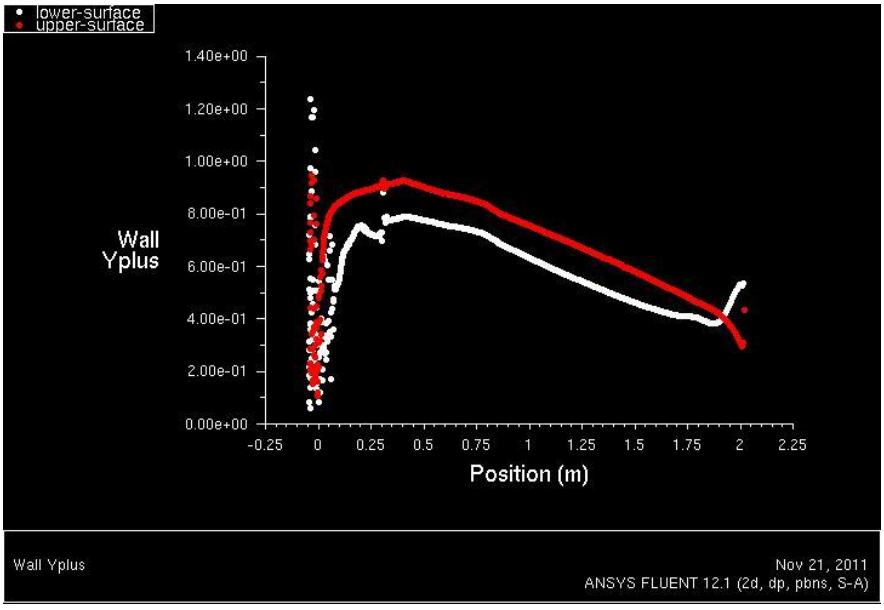

Figure 12. Wall y+ values on the airfoils upper and lower surfaces as a function of chord position in Case 2 for section 1.

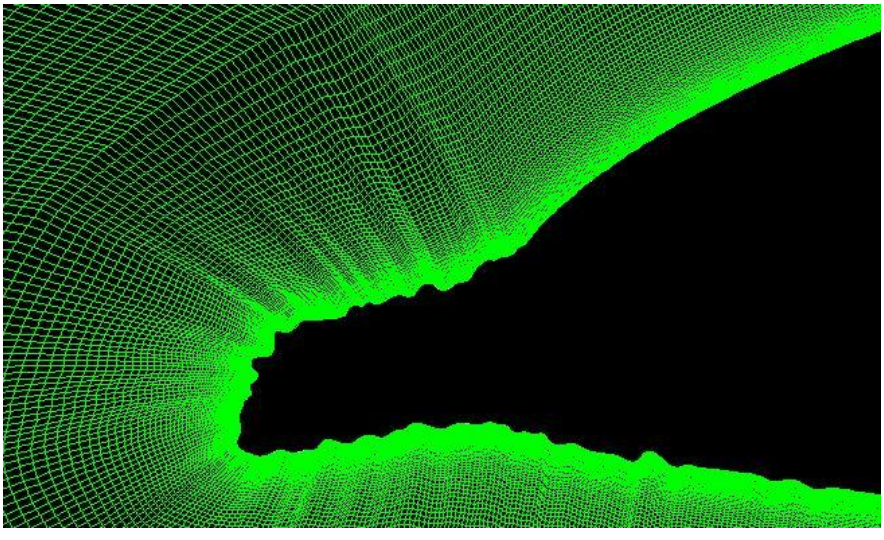

Figure 13. Grid on the leading edge of the airfoil in Case 3 for section 1.

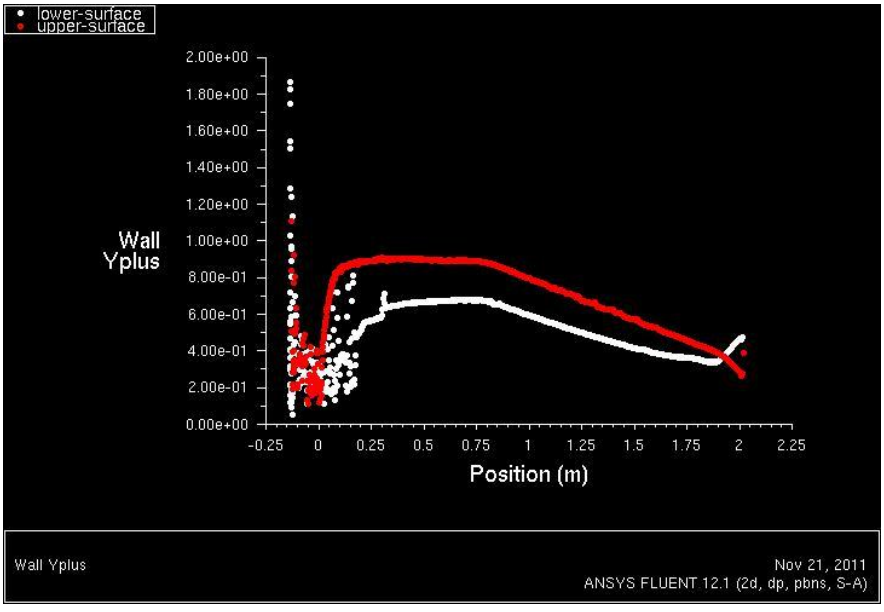

Figure 14. Wall y+ values on the airfoils upper and lower surfaces as a function of chord position in Case 3 for section 1.

4.3 CFD settings

Turbulence model used was one equation Spalart-Allmaras. Energy equation was applied and the air was considered to be ideal gas. Boundary condition on the far-field was set as pressure far-field, wall on the airfoil surface and interior elsewhere. Turbulent intensity was set on a value of 0.2 % and no-slip condition was applied on the wall. Clean airfoil chord was used as the reference length for all the cases and the solver used was pressure based. All the simulations were made in a 2D environment. Second order equations were used to solve for pressure, density, momentum, modified turbulent viscosity and energy. Initial conditions were set as described in Table 5, taking into account the varying parameters (reference length, angle of attack) for each simulation case.

Table 5. Input parameters for CFD simulation.

Air temperature		-7	°C
Air absolute viscosity		1.7×10^{-5}	kg/(ms)
	Section 1	*Section 3*	
Absolute air velocity	40.39 m/s	51.18 m/s	
Mach number	0.1235	0.1565	

4.4 Small-scale surface roughness modification method

Previous research has shown the large impact of small-scale surface roughness on the drag coefficient *(Abbott et al. 1959)*. As the effect of roughness was not included in the CFD simulations, it had to be included afterwards.

Drag coefficients were rectified by the method presented by Bragg *(1982)*. Bragg describes in detail a method to correct the drag coefficient values due to ice accretion and small-scale surface roughness. Airfoil analysis codes at the time were not able to handle the roughness that is present in icing cases of an airfoil. Same problem is encountered with several codes in CFD today, due to the relatively large-scale of surface roughness.

Ice shape effects on lift coefficient were first analysed with the code and the analytical method presented here was used for drag coefficient modification. Original method resolves the overall effect of accreted ice by combining the effect of ice shape and small-scale surface roughness. As the effect of ice shape was already known in this case, it was possible to retract the ice shape from the method and deploy only the section of surface roughness together with the CFD simulation results. Thereby, the modified method can be expressed by Equations (2) and (3).

$$\Delta C_D = 0.01\left[(-15.8) \times \ln\left(\frac{k}{c}\right) + 23.2\right] \tag{2}$$

$$C_{D_{iced}} = (1 + \Delta C_D) C_D \tag{3}$$

Small-scale surface roughness *k/c* was determined by the method of Shin et al. *(1994)* and the roughness is 1 mm for Section 1 and 0.9 mm for Section 3. C_D is the drag coefficient to be modified and it was withdrawn from CFD results.

4.5 Results

4.5.1 CFD simulation results

Main variables in the scope of this research are the force coefficients for lift and drag. They are plotted for each case and section as a function of an angle of attack in Figure 15 and Figure 16. Force coefficients were determined with angles of attack ranging from -6° to 10° with a spacing of 2 degrees. As mentioned before, surface roughness has not been taken into account in any of these results yet.

It can be seen in the Figure 15 that the ice shape itself and the large-scale surface roughness do not have significant effect on lift coefficient slope. Based on previous research, the most significant difference to be expected is the decrease in maximum lift coefficient *(Harold 2000)*. This trend can also be seen with the largest angles of attack in Figure 15 as the ice amount increases. According to Harold *(2000)*, small-scale surface roughness that was not included in this simula-

tion has more effect on drag coefficient than lift coefficient, and therefore the results of the lift coefficient from CFD simulation can be used in the power performance calculations directly. Relatively small effect on lift coefficient slope with moderate angles of attack, caused by rime ice, has also been demonstrated and compared with experimental data by Jasinski et al. *(1997)*.

Ice shape and large-scale surface roughness have more impact on drag coefficient as Figure 16 presents. The values of the drag coefficient can be seen to multiply due to the ice geometry and large-scale surface roughness. Values of drag coefficient increase further when the angle of attack deviates more from 0 degrees. Even though the effects of ice shape and large-scale surface roughness can already be seen, the significant importance of the small-scale surface roughness consideration has been highlighted earlier *(Dahlqvist 1997; Jasinski et al. 1997)*, and therefore the modification had to be done.

Some numerical problems were faced during two of the simulations and those can be seen as noticeably higher or lower values with respect to the overall trend of the curves. These values were fitted to the curve for future processing and the fitted curves can be seen in Figure 17 as well as the fitted simulation points.

Airfoils with ice accretion didn't stall at any simulated angle of attack, but the slope of the curve for different cases predicts the decrease of maximum lift coefficient. Velocity streamlines of the separation bubble on the leading and trailing edge of the airfoil in case 3 can be seen in Figure 18 and Figure 19, respectively.

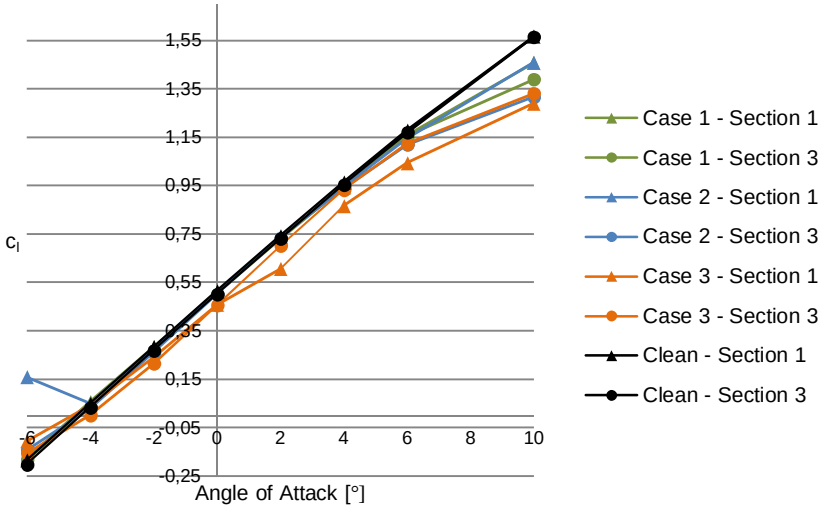

Figure 15. CFD results for lift coefficient for Case 1, Case 2, and Case 3.

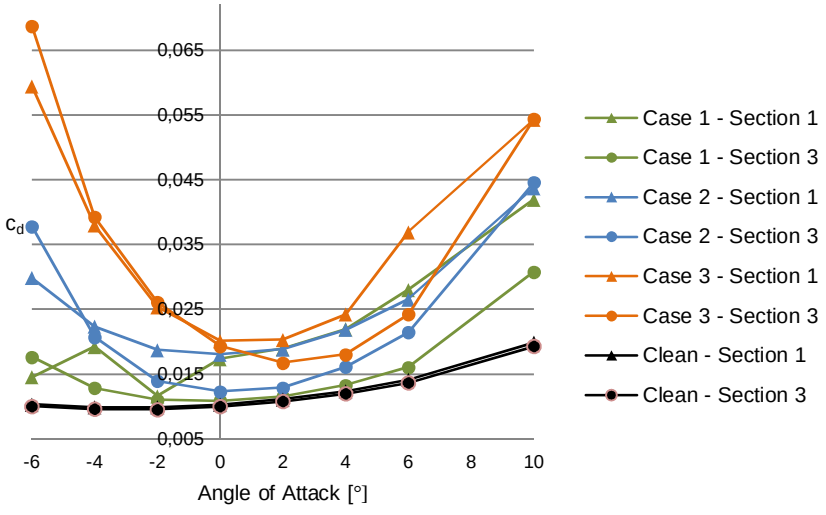

Figure 16. CFD results for drag coefficient for Case 1, Case 2 and Case 3.

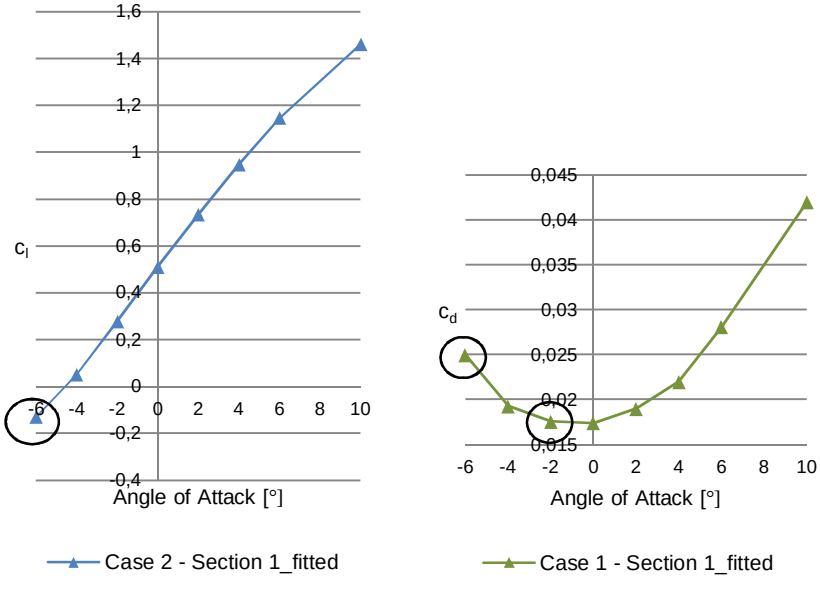

Figure 17. Fitted curves for lift coefficient of Case 2 Section 1 and drag coefficient for Case 1 Section 1. Fitted simulation points circled.

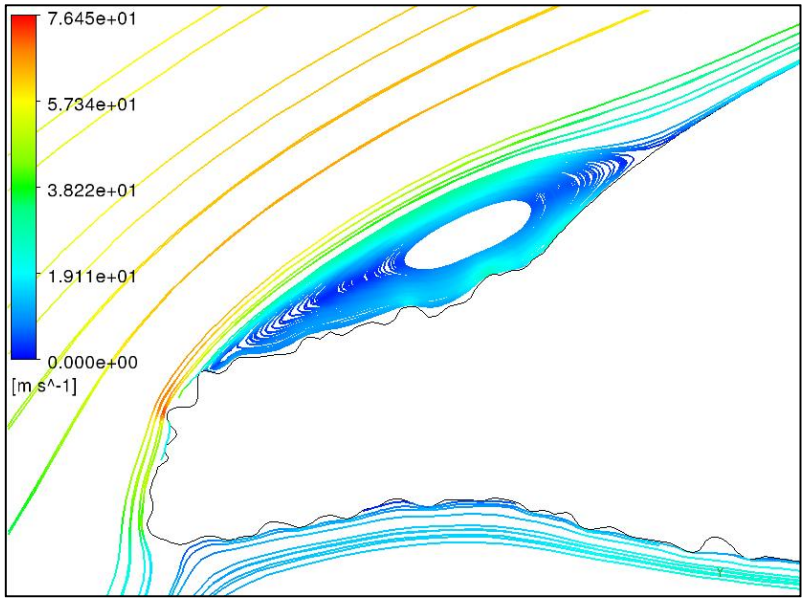

Figure 18. Streamlines of velocity on the leading edge in Case 3, Section 1 and angle of attack of 10 degrees.

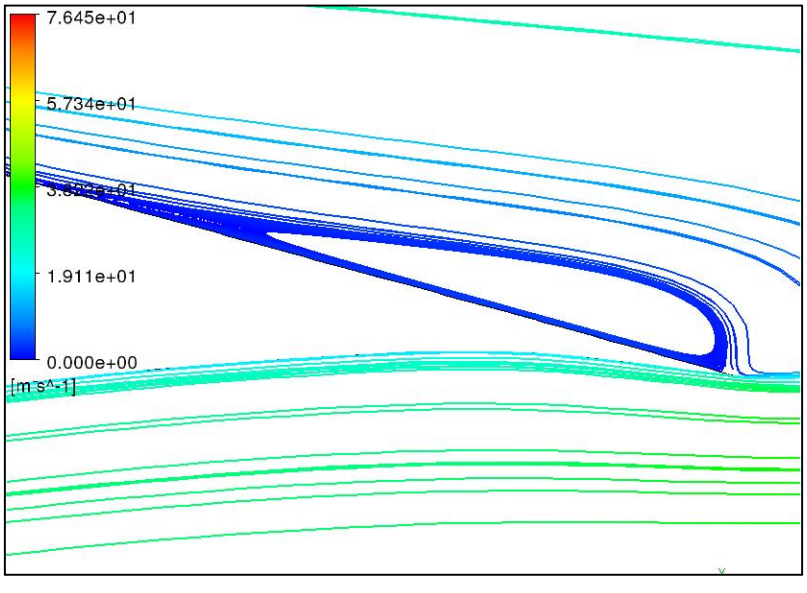

Figure 19. Streamlines of velocity on the trailing edge in Case 3, Section 1 and angle of attack of 10 degrees.

4.5.2 Small-scale surface roughness modification results

Small-scale surface roughness effects were taken into account next. After modifying the CFD results with the method described in Section 4.4, the new drag coefficient values were determined. Original CFD results and the modified new values can be seen in Figure 20 as a function of angle of attack for section 1. Drag coefficients increase significantly and the results are comparable with experimental results reported by Jasinski *(1997)*. Overall trend of the drag coefficient as a function of a lift coefficient, as presented in Figure 21, compares satisfactorily to experimental results.

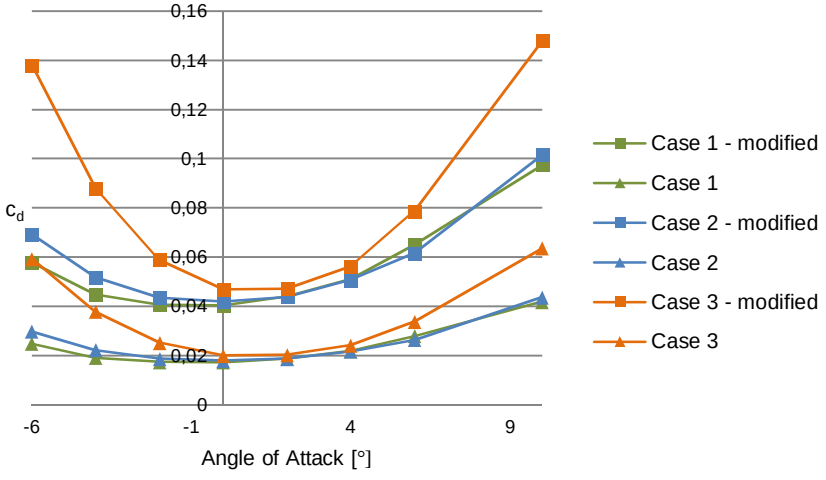

Figure 20. Original and rectified drag coefficient values for Section 1 in Case 1 (19 min), Case 2 (200 min) and Case 3 (600 min).

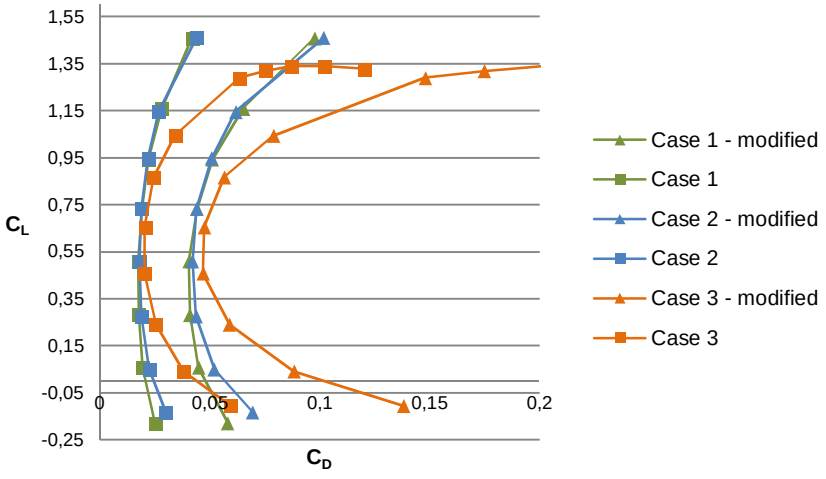

Figure 21. Original and modified drag coefficient values as a function of lift coefficient for section 1 in Case 1 (19 min), Case 2 (200 min) and Case 3 (600 min).

5. Power curve simulation

For the purposes of this work, a representative 3MW wind turbine model was constructed in FAST software *(Jonkman & Buhl 2005)*. It was used for simulating power curves corresponding to each icing case and a clean turbine as a reference case.

WinWinD WWD-3 wind turbine with 90 meter rotor was used in the Finnish Wind Atlas for production estimation *(Tammelin et al. 2011)*, and therefore similar turbine was used to determine the production losses in this study. WWD-3 is a variable speed pitch controlled 3 MW wind turbine. Because the exact rotor geometry was not available, the rotor geometry of NREL 5 MW wind turbine *(Jonkman et al. 2009)* was scaled down based on the rotor diameter to derive the blade geometry of the WWD-3 turbine. The blade geometry and other turbine parameters were tuned so that the simulated power curve for clean (non-iced) turbine corresponds to the WWD-3 power curve provided by the turbine manufacturer. The structural properties of the wind turbine were of minor importance in this study, and thus this approach was considered as adequate.

5.1 Aerodynamic input parameters

FAST requires lift and drag coefficient information for certain angles of attack for every specific rotor blade section. Lift and drag coefficients of iced airfoils were used as input. However, for Case 3 the lift and drag coefficients needed to be extrapolated for higher angles of attack, because the coefficients from CFD were not covering the whole range that was needed in Case 3 power curve simulation. Therefore the values were extrapolated for angle of attack values of 11°, 12°, 13°, 14° and 15°. Extrapolation was performed by hand by comparing the simulated lift and drag curves to similar curves presented vastly in literature. Both the lift and drag slope have a common shape that can be followed until the stall is reached. Stall was assumed not to occur yet at 15° angle of attack. Extrapolated lift and drag curves can be seen in Figure 22 and Figure 23, respectively.

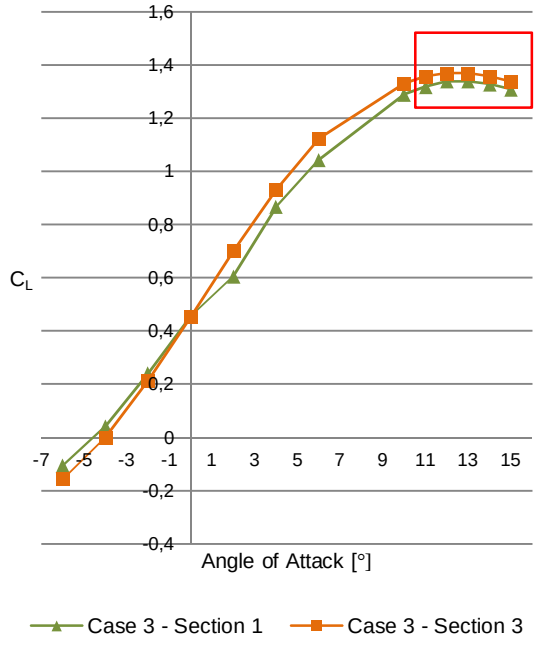

Figure 22. Extrapolated lift coefficient values for Case 3.

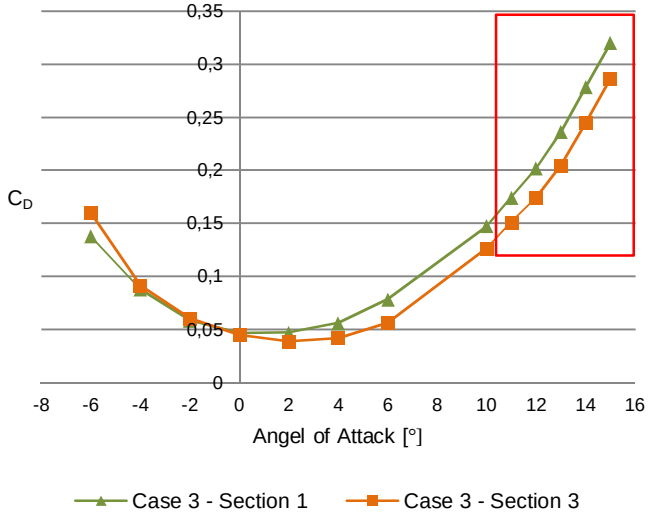

Figure 23. Extrapolated drag coefficient values for Case 3.

5.2 Results

The simulated power curves for each icing case are presented in Figure 24. The power losses as percentages are presented in Table 6.

The results show a significant drop in power production due to small-scale surface roughness in Case 1. However, a slight increase in ice mass in Case 2 does not seem to affect the production loss very much compared to Case 1. Larger ice shape in Case 3 has a greater impact. It is worth noting that with rime ice, most of the production losses are due to the increased drag. The decreased maximum value of the lift coefficient has an effect as well, but it does not show as clearly in the power curves as the drag effect.

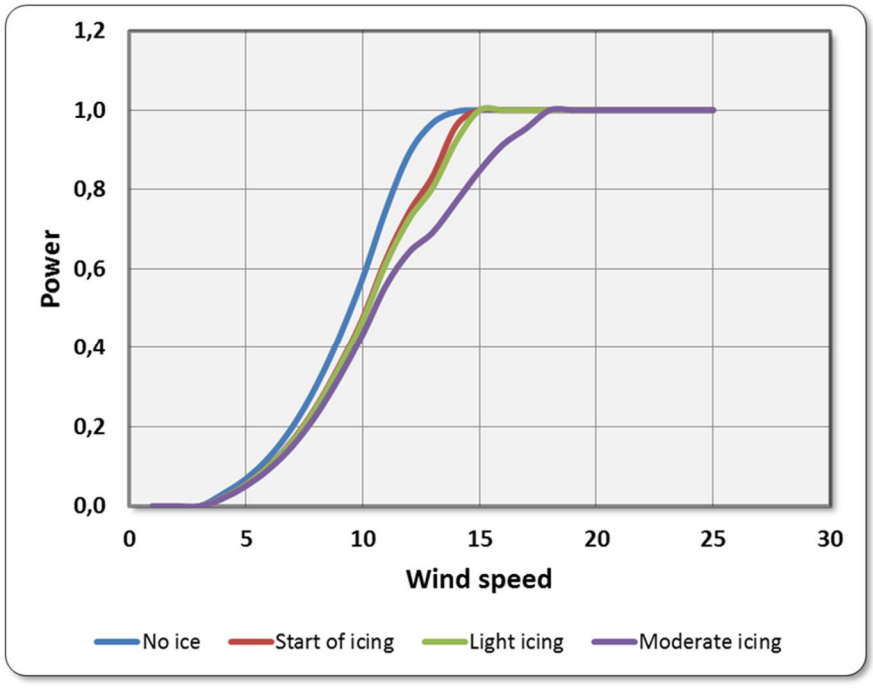

Figure 24. Power curves of each icing cases and a clean wind turbine (no ice) as a reference.

Table 6. Power losses as percentages for different ice cases in comparison to no-ice case.

Wind speed	**Icing case**		
[m/s]	Start of icing	Light icing	Moderate icing
4	31 %	33 %	36 %
5	20 %	22 %	26 %
6	17 %	18 %	24 %
7	17 %	18 %	24 %
8	17 %	18 %	24 %
9	17 %	18 %	24 %
10	18 %	19 %	25 %
11	17 %	18 %	26 %
12	17 %	19 %	28 %
13	14 %	17 %	29 %
14	4 %	8 %	23 %
15	0 %	0 %	15,2 %
16	0 %	0 %	8,7 %
17	0 %	0 %	4,6 %
18	0 %	0 %	0 %
19	0 %	0 %	0 %
20	0 %	0 %	0 %
21	0 %	0 %	0 %
22	0 %	0 %	0 %
23	0 %	0 %	0 %
24	0 %	0 %	0 %
25	0 %	0 %	0 %

6. Discussion and conclusions

Power loss estimates for three different rime ice cases were determined for a 3 MW wind turbine. Results show decreasing production levels for iced up turbine. Main cause for the lower production levels was noticed to be the small-scale surface roughness that increases drag significantly. Therefore, power production drops already early in the icing process due to the accumulated roughness. When the icing times are longer, more ice mass accretes on the blade changing the geometry of the airfoil. Accreted ice shapes further increase the drag and also the maximum lift coefficient is reduced.

The study shows that the prediction of icing events and their severity is important for estimating the power production of the wind turbines. However, there are certain parameters to consider when interpreting results presented here. For example, only rime ice cases have been simulated, whereas glace ice shapes are more complex and thus potentially cause bigger aerodynamic penalties and production losses. Glace ice is known to form with temperatures just below zero degrees Celsius and, therefore, it can also occure in Finnish meteorological conditions. Thus the resulted power curve estimates in this study can be considered higher in power than what might be observed in real life.

Also the weather parameters were selected for one representative rime ice case only. Varying these parameters might have caused slight variation in the results. However, within this report only one representative case was required.

Some uncertainties are always included in simulating real-life events. In this study, particulary, the modifications performed based on figures and reported information need to be taken into account. The large-scale surface roughness and its geometry are not fully reproducible. Even though the examples of experimental ice shapes were used, the effect of modification cannot be neglected. This also applies to the extrapolated values of the lift and drag coefficients.

Acknowledgements

This study was carried out under the project IEA Wind 2009 – 2011, which was funded by TEKES - the Finnish Funding Agency for Technology and Innovation, EPV, Fortum, Hoxville, Innopower, Labkotec, Vaisala, Winwind, WPD Finland, and VTT, and under the project Icewind, which was funded by VTT and Nordic Energy Council through Nordic Top-level Research Initiative.

The authors greatly acknowledge the cooperation with FMI and VTT Industrial CFD team.

References

Abbott, I.H. & von Doenhoff, A.E. 1959. Theory of Wind Sections. Dover Publications, Inc. New York.

Bragg, M.B. 1982. Rime Ice Accretion and Its Effect on Airfoil Performance. NASA Contractor Report 165599. National Aeronautics and Space Administration, Lewis Research Center.

BTM Consult ApS. March 2011. International Wind Energy Development – World Market Update 2010. ISBN 978-87-991869-5-2.

Burton, T., Sharpe, D., Jenkins, N. & Bossanyi, E. 2001. Wind Energy Handbook. Wiley.

Dahlqvist, A. 1997. The Effects of Ice on the Aerodynamics of the Rotor Blades of a Wind Turbine. Master's thesis. Helsinki University of Technology, Department of Mechanical Engineering. Espoo.

Finnish Icing Atlas. 2012. Finnish Meteorological Institute. *[Cited 26.6.2013]* Available at: http://tuuliatlas.fmi.fi/en/.

Harold, E.A. Jr. 2000. Ice Accretions and Icing Effects for Modern Airfoils. TP-2000-210031. National Aeronautics and Space Administration. Glenn Research Center.

Homola, M.C., Virk, M.S., Wallenius, T., Nicklasson, P.J. & Sundsbø, P. A. 2010. Effect of atmospheric temperature and droplet size variation on ice accretion of wind turbine blades. Journal of Wind Engineering and Industrial Aerodynamics, Vol. 98, pp.724–729.

ISO 12494. 2001. Atmospheric icing of structures. Geneva, ISO. 56 p.

Jasinski, W.J., Noe, S.C., Selig, M.S. & Bragg, M.B. 1997. Wind turbine performance under icing conditions. AIAA Paper 97-0977. American Institute of Aeronautics and Astronautics, Inc.

Jonkman, J. & Buhl, M.L. Jr. 2005. FAST User's Guide. Technical Report. NREL/EL-500-38230. National Renewable Energy Laboratory.

Jonkman, J., Butterfield, S., Musial, W. & Scott, G. 2009. Definition of a 5-MW Reference Wind Turbine for Offshore System Development. Technical Report, NREL/TP-500-38060. National Renewable Energy Laboratory.

Makkonen, L., Laakso, T., Marjaniemi, M. & Finstad, K.J. 2001. Modelling and prevention of ice accretion on wind turbines. Wind Engineering, Vol. 25, No. 1, pp. 3–21.

Mortensen, K. 2008. CFD Simulations of an Airfoil with Leading Edge Ice Accretion. Master's thesis. Technical University of Denmark, Department of Mechanical Engineering. Lyngby.

Shin, J., Berkowitz, B., Chen, H.H. & Cebeci, T. 1994. Prediction of Ice Shapes and Their Effect on Airfoil Drag. Journal of Aircraft, Vol. 31, Issue 2, pp. 263–270.

Tammelin, B., Vihma, T., Atlaskin, E., Badger, J., Fortelius, C., Gregow, H., Horttanainen, M., Hyvönen, R., Kilpinen, J., Latikka, J., Ljungberg, K., Mortensen, N.G., Niemelä, S., Ruosteenoja, K., Salonen, K., Suomi, I. & Venäläinen, A. 2011. Production of the Finnish Wind Atlas. Wind Energy. Research article. *[Cited 29.3.2012]*. DOI: 10.1002/we.517.

US Department of Energy. 2012. National Renewable Energy Laboratory; US installed capacity 2008. *[Cited 29.3.2012]*. Available at: http://www.windpoweringamerica.gov/wind_installed_capacity.asp.

VTT Technical Research Center of Finland. 2012. Finnish wind power statistics. *[Cited March 2012]*. Available at: http://www.vtt.fi/proj/windenergystatistics/?lang=en.

Series title and number
VTT Technology 114

Title	**Method for estimating wind turbine production losses due to icing**
Author(s)	Ville Turkia, Saara Huttunen & Tomas Wallenius
Abstract	Atmospheric icing causes production losses to wind turbines, poses a risk of ice throw and increases dynamic loading of wind turbine which might reduce the lifetime of turbine components. These effects are qualitatively widely known but not quantitatively. In order to estimate effects of icing to power production of a typical 3 MW wind turbine, a simulation based study was made. Three rime ice cases were selected with the meteorological conditions typical for Finnish climate. Conditions were the same for each case. The lengths of the icing events were varied to represent different phases of an icing event; beginning of icing, short icing event and long lasted icing event. Thus, three different ice masses accreted on a wind turbine blade were simulated. Accretion simulations were performed with a VTT inhouse code TURBICE. The aerodynamical properties of the iced profiles were modelled using computational fluid dynamics (CFD) with ANSYS FLUENT flow solver. As a result, lift and drag coefficients were drawn as a function of an angle of attack. Small-scale surface roughness effect on drag coefficient was determined analytically. Finally, the power curves were generated with FAST software for the clean wind turbine and for the same turbine with the different ice accretions. The results showed relatively large impact of small-scale surface roughness on power production. In the beginning of an icing event, where ice causes basically only increased surface roughness, power production was discovered to reduce by approximately 17 % below rated wind speeds compared to the no-ice case. As the ice mass was increased, production reduction was 18 % for short icing event and 24 % for long lasted icing event. However, the relative reduction was smaller than in the beginning of icing, mainly due to the small-scale surface roughness that remained at the same level. The results indicate that the surface roughness is crucial to take into account when defining the aerodynamic penalty caused by icing of wind turbine blades. The generated power curves for iced up wind turbine in this study estimate higher power production than can be expected from the observations in real life. This is caused by the less complex ice shapes resulting from simulating only rime ice conditions. The results of this study were used in the Finnish Icing Atlas *(2012)*, where time dependent numerical weather simulations were carried out to calculate icing conditions and energy production losses. The results were also used in ICEWIND project for production loss estimation process.
ISBN, ISSN	ISBN 978-951-38-8041-5 (URL: http://www.vtt.fi/publications/index.jsp) ISSN-L 2242-1211 ISSN 2242-122X (Online)
Date	August 2013
Language	English, Finnish abstract
Pages	38 p.
Name of the project	
Commissioned by	
Keywords	Icing, wind turbine, production loss, simulation, rime ice, icing atlas
Publisher	VTT Technical Research Centre of Finland P.O. Box 1000, FI-02044 VTT, Finland, Tel. 020 722 111

Julkaisun sarja ja numero
VTT Technology 114

Nimeke	**Menetelmä jäätymisen aiheuttamien tuuliturbiinin tuotantotappioiden arviointiin**
Tekijä(t)	Ville Turkia, Saara Huttunen & Tomas Wallenius
Tiivistelmä	Tuulivoimaloiden lapoihin kertyvä jää aiheuttaa tuulivoimaloille tuotantotappioita, aiheuttaa jäänlentoriskin ja kasvattaa tuulivoimalan komponenttien väsymiskuormia, jotka voivat johtaa komponenttien eliniän lyhenemiseen. Nämä jäätämisen haittavaikutukset tunnetaan laajalti, mutta niiden suuruutta on ollut vaikea arvioida. Tässä tutkimuksessa arvioidaan jään aiheuttamaa tehon alenemaa tyypilliselle 3 MW tuulivoimalalle simuloinnin keinoin. Kolme Suomen ilmastolle tyypillistä jäätämistapausta valittiin edustamaan oleellisinta osaa tuotantotappioita aiheuttavista jäätämistilanteista. Meteorologiset suureet olivat samat jokaiselle tapaukselle, mutta jäätämistilanteiden kestoa kasvatettiin, jotta voitiin kuvata jäätämisen alkuvaihe sekä lyhyehkö ja pitkään jatkunut jäätämistilanne. Nämä kolme jäätämistilannetta simuloitiin VTT:n omalla TURBICE-ohjelmalla. Aikaansaatujen kolmen jäämuodon aerodynaamiset ominaisuudet mallinnettiin laskennallisen virtausmekaniikan (CFD) keinoin käyttäen ANSYS FLUENT ohjelmaa. Pinnankarheuden vaikutus vastukseen määriteltiin erikseen analyyttisellä menetelmällä. Lopulta esimerkkituulivoimalan tehokäyrät simuloitiin FAST-ohjelmalla puhtaalle tuulivoimalalle ja kolmelle jäätymistapaukselle. Tulokset osoittivat pinnankarheuden vaikuttavan tehontuotantoon verrattain paljon. Jäätämisen alkuvaiheessa käytännössä ainoastaan tuulivoimalan lavan pinnankarheus muuttuu, mikä johti noin 17 % tehon alenemaan toimittaessa alle nimellistuulennopeuden. Jään massan kasvaessa tehon alenema kasvoi edelleen 18 %-yksikköön lyhyehköllä jäätämistapauksella. Pitkään jatkuneella jäätämistapauksella tehon alenema oli 24 %, mutta muutos oli suhteellisesti pienempää, sillä pinnankarheus pysyi samansuuruisena. Tulokset osoittavat, että pinnankarheuden huomioon ottaminen on erittäin tärkeää määriteltäessä jäätyneiden tuulivoimalan lapojen aerodynaamisia ominaisuuksia. Tässä tutkimuksessa lasketut tehon alenemat ovat pienempiä verrattuna joihinkin todellisiin havaintoihin, sillä jäämuodot laskettiin vain huurrejäätapauksille, joissa jään muodot eivät ole yhtä monimutkaisia kuin ne tosielämässä voivat olla. Tämän työn tuloksena saatuja tehokäyriä käytettiin Suomen Jäätämisatlaksessa, jossa numeerisella sääennusteohjelmalla simuloitiin sääolosuhteita ja laskettiin jäätämisolosuhteita sekä jäätämisen aiheuttamia tappioita energiantuotantoon. Tuloksia hyödynnettiin myös ICEWIND-projektissa tuotantotappioiden arvioinnissa.
ISBN, ISSN	ISBN 978-951-38-8041-5 (URL: http://www.vtt.fi/publications/index.jsp) ISSN-L 2242-1211 ISSN 2242-122X (verkkojulkaisu)
Julkaisuaika	Elokuu 2013
Kieli	Englanti, suomenkielinen tiivistelmä
Sivumäärä	38 s.
Projektin nimi	
Toimeksiantajat	
Avainsanat	Icing, wind turbine, production loss, simulation, rime ice, icing atlas
Julkaisija	VTT PL 1000, 02044 VTT, Puh. 020 722 111

Method for estimating wind turbine production losses due to icing

IISBN 978-951-38-8041-5 (URL: http://www.vtt.fi/publications/index.jsp)
ISSN-L 2242-1211
ISSN 2242-122X (Online)

VTT TECHNOLOGY 114 Method for estimating wind turbine production losses due to icing